Journal of Oceanology and Limnology
Vol. 40 No. 3, P. 969-985, 2022
https://doi.org/10.1007/s00343-021-1112-z

Geochemical characteristics of cold-seep carbonates in Shenhu area, South China Sea*

Chongmin CHEN[1], Lifeng ZHONG[2, **], Zhifeng WAN[1, 2, **], Chiyu CHENG[1], Wei ZHOU[2], Xing XU[3]

[1] *School of Marine Sciences, Guangdong Provincial Key Laboratory of Marine Resources and Coastal Engineering, Sun Yat-sen University, Zhuhai 519000, China*

[2] *Southern Marine Science and Engineering Guangdong Laboratory (Zhuhai), Zhuhai 519000, China*

[3] *MLR Key Laboratory of Marine Mineral Resources, Guangzhou Marine Geological Survey, Ministry of Natural Resources, Guangzhou 510075, China*

Received Apr. 21, 2021; accepted in principle Jun. 16, 2021; accepted for publication Jul. 23, 2021

Abstract Cold seeps spread worldwide along the continental margins, which are closely related to the exploration of gas hydrates. Cold-seep carbonates have been reported to record the nature of seepage, including fluid source, sedimentary environment, and variation of seepage activity. We investigated the morphology, mineralogy, element compositions, and carbon and oxygen isotopes of 15 cold-seep carbonates collected from the Shenhu area, and compared them with 2 carbonates from the Haima cold seep, the South China Sea (SCS), to promote our knowledge of cold-seep system in SCS. Most of the Shenhu carbonates exhibit crust morphology, and some are in the form of chimneys and blocks. Their absolute (20%–65%) and relative carbonate mineral contents (mainly aragonite and calcite, with minor samples containing dolomite) vary significantly, indicating the multi-stage methane leakage in our study area. Some samples show a slight negative Ce anomaly, suggesting either the mixing of seawater or variation of the redox condition during the precipitation; the co-occurrence of strongly enriched U and Mo demonstrates anoxic condition during precipitation. The mixed genetic methane source was interpreted by $\delta^{13}C$ of the Shenhu carbonates to range from -22.34‰ to -59.30‰ Vienna PeeDee Belemnite (VPDB), and the slight ^{18}O-enrichment imprinted on the carbonates suggests the possible influence from hydrate dissociation. The Haima carbonates, with biogenic methane as the main gas source, were presumably formed in a stronger fluid flux by compared with our Shenhu samples.

Keyword: cold-seep carbonates; geochemistry; sedimentary environment; fluid source; Haima cold seep; Shenhu area; South China Sea

1 INTRODUCTION

Cold seeps, a phenomenon of natural fluid leakage, are formed by the upward migration of fluids mainly composed of water, hydrocarbon, hydrothion, and fine-grained sediments (Joseph, 2017) and generally related to the dissociation of gas hydrates (Chen and Cathles, 2005; Feng and Chen, 2015) or the upward migration of gas and oil beneath the seafloor along geologically weak zones, which are widely distributed around the world and play an indicative role in the deep exploration of oil and gas (Suess, 2014; Feng et al., 2018).

Seeps are closely connected to material circulations (such as carbon and sulfur etc.) and of great importance to trace the deep origin of life (Boetius and Wenzhöfer, 2013; Suess, 2014). Typically characterized by rich methane, cold seeps play a crucial role in reconstructing paleoclimate and detecting deep hydrocarbon resources (Feng et al., 2018). Each cold seep presents its unique nature as it is heterogeneous both in time and space, stressing the necessity of specific and regional research on cold seep.

* Supported by the Guangdong Province Marine Economic Development (Six Major Marine Industries) Special Fund Project (No. [2021] No. 58), the National Key R&D Program of China (No. 2018YFC0310000), and the National Natural Science Foundation of China (Nos. 41776056, 42076054)
** Corresponding authors: zhonglifeng@sml-zhuhai.cn; wanzhif@mail.sysu.edu.cn

After the first discovery at a depth of 3 200 m on the Florida cliff in the Gulf of Mexico (Paull et al., 1984), cold seeps and cold-seep carbonates were found in both active and passive continental margins (Suess, 2014; Feng et al., 2018). To date, cold seeps have been found from the tropics to the poles, and from shallow continental shelves to abyssal plains or trenches (Roberts and Aharon, 1994; Campbell, 2006; Roberts et al., 2010; Suess, 2014).

During the upward migration of cold-seep fluid, methane in the fluid and sulfate diffusing downward into the sediments cause anaerobic oxidation of methane (AOM) and sulfate reduction reactions (Eq.1) (Reeburgh, 2007).

$$CH_4+SO_4^{2-}\rightarrow HCO_3^-+HS^-+H_2O, \quad (1)$$

$$2HCO_3^-+Ca^{2+}\leftrightarrow CaCO_3+CO_2+H_2O. \quad (2)$$

Under the joint action of methane-oxidizing archaea and sulfate-reducing bacteria, the alkalinity of the surrounding fluid increases, causing methane-derived carbonate to locally supersaturate and form authigenic carbonate in the sulfate methane transition zone (SMTZ) (Eq.2) (Raiswell, 1988; Chen et al., 2015; Peketi et al., 2015).

Cold-seep carbonate is an important product of cold seep in shallow seafloor burial, whose morphology, mineralogy, and other characteristics contain abundant information of cold seep (Chen et al., 2005; Suess, 2005; Han et al., 2008). Researches on cold-seep carbonates have revealed the distribution and activity of cold seeps in geological history and the interaction between the formation environment of cold-seep carbonates and surrounding environment, especially in the case of paleo-cold seeps wherein fluid activity ceased (Naehr et al., 2007; Feng and Chen, 2015; Yang et al., 2018). Further investigation is required to explore the characteristics of fluid evolution in response to the geochemical characteristics of different occurrences. In addition, the carbon and oxygen isotopes of cold-seep carbonates vary across different sea areas, reflecting the variations in fluid leakage rates and sedimentary environment of cold-seep fluids from different sources (Chen et al., 2005; Han et al., 2008, 2014; Tong et al., 2013; Feng and Chen, 2015; Liang et al., 2017; Feng et al., 2018). Trace elements, especially redox-sensitive elements (e.g. Mo, U, Cr, Co) and the rare earth elements (REE) of cold-seep carbonates, show great potential to help reconstruct the paleo-environment (Ge et al., 2010; Smrzka et al., 2020).

Shenhu area where the first hydrate trial situated in the South China Sea (SCS) is a vital platform for hydrate and cold-seep research in China. In 2004, several cold-seep carbonates were detected by China's *Haiyang-4* ("ocean" in Chinese) vessel in this sea area where gas hydrate samples were extracted thereafter; and the first trial production of gas hydrate was successfully completed with a total gas production of 309 000 m^3 in July 2017, which strongly proved the significance of cold-seep activities in the development of gas hydrates (Suess, 2005; Zhang et al., 2007, 2019). Studies have shown that different sedimentary environments and fluid evolution characteristics tend to produce cold-seep carbonates with various morphological characteristics, mineral compositions, and geochemical characteristics (Feng et al., 2009; Han et al., 2013; Lu et al., 2015). Previous studies on cold-seep carbonates in this area focused on the geochemical characteristics of fluid, biomarkers, and fluid evolution of chimney-shaped cold-seep carbonates (Ge et al., 2010; Feng et al., 2018; Zhang et al., 2019).

A large, active submarine cold seep, named Haima cold seep, was discovered by the remotely operated vessel (ROV) *Haima* ("hippocampus" in Chinese) in 2015 and named after the ROV name. The Haima cold seep is abundant in authigenic carbonates, exposed gas hydrates, and widely developed cold-seep biota (Liang et al., 2017; Feng et al., 2018).

Here, we firstly observed and described the morphology of the cold-seep carbonates from Shenhu area and then carried out a detailed study on the mineralogical and geochemical characteristics (element compositions and isotopes of carbon and oxygen) of the carbonates from Shenhu. Focusing on Shenhu area, we further compare Shenhu cold-seep carbonates with those from Haima cold seep, in order to understand the regional specificity of Shenhu cold-seep activities, meanwhile, to demonstrate the necessity of more detailed cold-seep research in various regions, especially in the SCS (known as its complex tectonic settings).

2 GEOLOGICAL SETTING

Shenhu area is located in the Baiyun Sag of the Zhuer Depression of the Zhujiang (Pearl) River Mouth Basin (Fig.1), which is in the transition zone between the northern continental slope and the Central Sea Basin of the SCS. The seabed has a highly undulating topography with various geomorphic types, such as sea valleys, domes, and erosion grooves, with water depth in the range of 1 000–3 000 m, water temperature of 3.3–3.7 °C, and

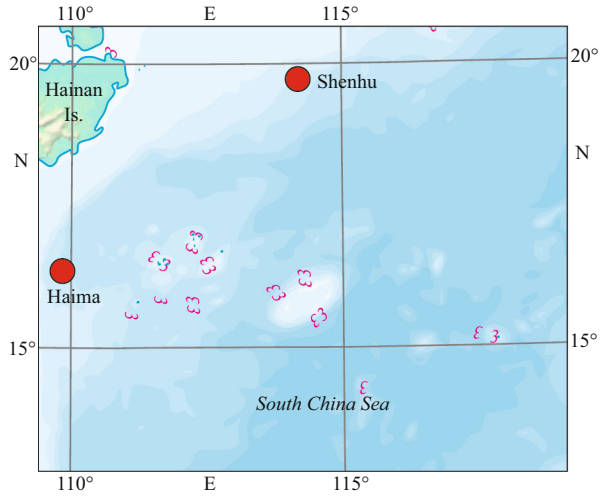

Fig.1 The study areas (red circle) include Shenhu area and the Haima cold seep near Hainan Island in northern South China Sea

geothermal gradient of 45–67.7 °C/km (Su et al., 1989; Yu, 1990; Zhang et al., 2018). Rich oil and gas resources have been discovered in this area (He et al., 2009; Li et al., 2016). The neotectonics led to the formation of a large active diapir belt, while fluid discharge and overflow occurred on the seabed, resulting in the abnormal development of mud diapirs and gas chimneys and the formation of arch anticlines at different depths, which provided fluid passages for the migration of gas hydrates (Ge et al., 2010; Wu et al., 2010; Liang et al., 2014; Su et al., 2018).

The Haima cold seep is located in the uplift zone of the Qiongdongnan Basin in the northwestern region of the SCS (Gong et al., 1997; Xie et al., 2006). The combination of thick sedimentary sequence and high geothermal gradient, coupled with faults or diapirs, significantly promoted the generation and migration of natural gas in the basin (Sun et al., 2017). Bottom-simulating reflectors (BSR) and gas chimneys are widely distributed at the bottom of the basin, which further indicates the presence of gas hydrates in the area (Hui et al., 2016; Liang et al., 2017).

3 MATERIAL AND METHOD

A total of 17 samples were investigated in this study. 15 samples were from Shenhu area (SH2017-1–SH2017-15) and were obtained during the 2017 survey trawl (China's *Haiyang-4* vessel, the Guangzhou Marine Geological Survey). The Shenhu samples were collected at water depths of 500–700 m. The other 2 samples (ROV2 and ROV12) from the Haima cold seep were collected from the seabed by the ROV of China's *Haiyang-6* in 2015. In the study area of Haima cold seep, the temperature of bottom water was 3.0 °C, and the water depth was approximately 1 370–1 390 m.

All samples were washed with seawater, dried naturally, and stored at room temperature (25 °C) in the Key Laboratory of Marginal Sea and Oil and Gas Exploration, School of Marine Science, Sun Yat-sen University. The morphological characteristics of each sample were observed, photographed, and recorded in detail.

The X-ray diffraction (XRD) analysis of the carbonates was carried out at the School of Chemistry, Sun Yat-sen University. Firstly, small pieces were cut from the fresh surface of the samples and were ground to powder less than 200 meshes using an agate mortar. Then, a Bruker D8 Advance X-ray diffractometer was used for the analysis. The parameters were set as Cu target Kα ray, power of 40 kV/30 mA, 2θ scanning range of 3°–85°, incidence slit of 1 mm, and scanning speed of 4°/min. The MDI Jade9 software was used to analyze the d values and relative strength of the obtained XRD spectra to determine the mineral composition. Meanwhile, according to the ratios of the maximum diffraction peaks of the minerals obtained in the XRD spectra to the maximum diffraction peaks of the standard minerals, the percentage contents of the main minerals were semi-quantitatively determined, and the analysis accuracy was ±5 weight (wt.)%.

The analysis of major and trace elements (including REE) was done at the University of Queensland, Australia. The procedure is as follows. First, about 200-mg samples were weighed and placed in a Teflon centrifuge tube, then washed twice with 2-mL MilliQ water. Two milliliter acetic acid was then added in and sonicated for 1 h, followed by heated at 80 °C for 12 h for complete dissolution. After centrifugation, the supernatant was collected into a pre-cleaned Teflon beaker. After the supernatant was dried up at 120 °C, 2-mL 7-mol/L HNO_3 was added. Upon fully dissolution followed by dry-down again, 2-mL 1-mol/L HNO_3 was added for dissolution for 12 h. Then, 50-μL solutions were extracted and added with 0.5-mL internal standard and 4.45-mL 2% HNO_3, which were all precisely weighed. After centrifugating for 10 min, the major and trace elements of sample solution were analyzed on Agilent 7900 inductively coupled plasma-mass spectrometry (ICP-MS). BHVO-2, W-2, and JCP-1 were used as calibration standards and BIR-1 as cross check. The enrichment factor (EF) of trace elements in carbonates was calculated by X_{EF}=[(X/

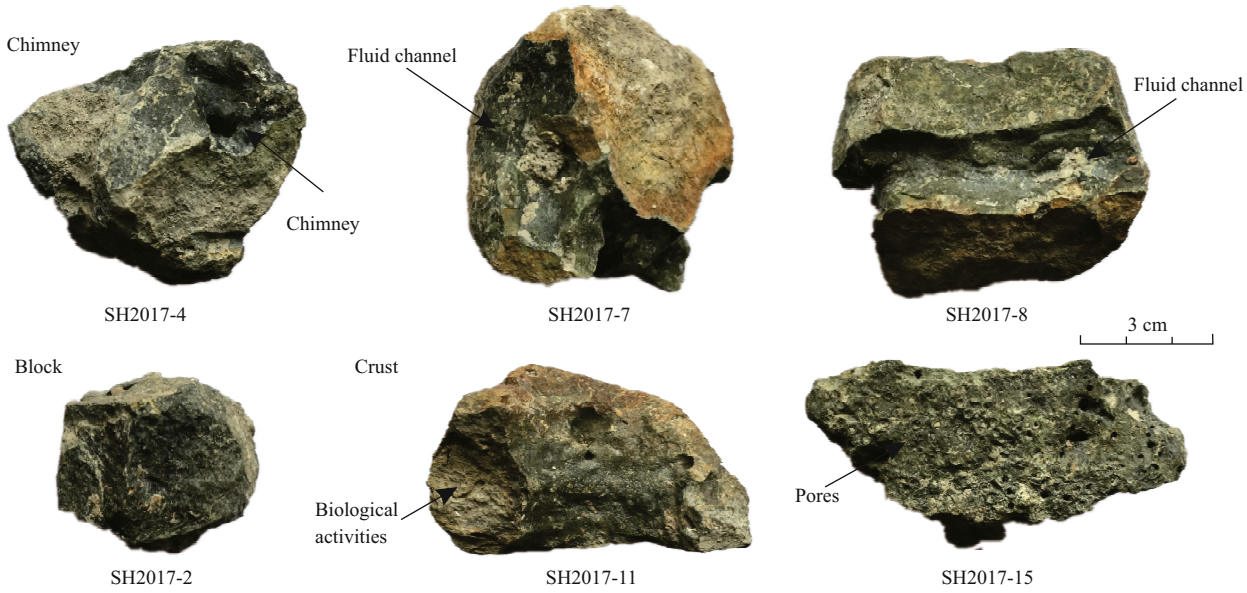

Fig.2 Representative cold-seep carbonate samples from the Shenhu area

The morphology of the samples is described as chimney, block, and crust based on their appearance. Obvious evidence of fluid migration is shown on samples 7 and 8. Traces of biological activity are also evident, such as that shown on sample 11.

Ti)$_{sample}$/(X/Ti)$_{PAAS}$], where X represents the index element and PAAS represents the standardization of the Post Archean Australian Shale (PAAS; McLennan, 1989). Al in pelagic seawater will be scavenged by organic matter, so it may be unsuitable to use Al to represent terrestrial sediments here (Murray and Leinen, 1996). Therefore, Ti was used in this study to replace Al as the standard of terrestrial sediments. Enrichment factors can be used effectively to evaluate the degree of autogenous enrichment of trace elements (Tribovillard et al., 2006). Generally, an enrichment factor greater than 1 indicates enrichment relative to the standard, an enrichment factor greater than 3 indicates detectable enrichment, and an enrichment factor greater than 10 indicates moderate to strong enrichment (Algeo and Tribovillard, 2009).

In this paper, Ce/Ce*=2Ce$_N$/(La$_N$+Nd$_N$). Log(Ce/Ce*) stands for Ce anomaly. Eu/Eu*=2Eu$_N$/(Sm$_N$+Gd$_N$), Pr/Pr*=2Pr$_N$/(Ce$_N$+Nd$_N$), where the subscripted N represents the relative value of the standardization of PAAS (McLennan, 1989).

The measurements of carbon and oxygen isotopic compositions were also done at the University of Queensland, Australia. The powder samples reacted with 105% orthophosphoric acid at 90 °C to release CO_2 in the Dual Inlet system and Multiprep on-line sampler system. The product of CO_2 was imported into IsoPrime 100 mass spectrometer. The results were presented relative to VPDB standard. Analytical precision of C isotope and O isotope was better than 0.08‰ and 0.10‰, respectively.

4 RESULT

4.1 Hand specimen observation

The 15 cold-seep carbonates collected from Shenhu area (Fig.2) are numbered as SH2017-1–SH2017-15 (represented by 1–15 in this paper). Most of the samples are bluish-black with irregular crust form or in the form of chimneys and blocks. Yellowish-gray surface of some samples show obvious oxidized features, holes, and biological debris. Crust cement is visible in several samples. Samples 1, 4, 7, 8, and 10 appear as a chimney. The diameters of the central fluid channel and the outer ring of sample 1 with an evident arc-shaped cross section, are approximately 3 cm and 7 cm, respectively, which shows the traces of biological activities. Sample 4 has a central fluid channel with a diameter of 2 cm and contains bioclasts. Sample 10 has the most complete chimney shape with a diameter of about 3 cm. There are clear bluish-gray fluid migration channels without obvious cement features shown on samples 7 and 8.

Sample 2 is a compact block with crust cement on the surface.

Other samples are described as crust with the length of 6.5–10.5 cm. Millimeter-sized holes are observed on the surface of samples 3, 9, and 15, while sample 6 is darker than other samples exhibits large pores. Sample 9 presents cement and also channels for fluid migration shown on its cross section. Sample 11 also has crust cement and traces of tubular biological

Table 1 Some elements and carbonate content of carbonate samples

Sample	Description	Carbonate content (%)	MgO (%)	Fe_2O_3 (%)	MnO (%)	TiO_2 (μg/g)	Sr (μg/g)	Ni (μg/g)	Zn (μg/g)	Ba (μg/g)	Mo (μg/g)	U (μg/g)
Shenhu area												
SH2017-1	Chimney	50	7.25	0.14	0.29	3.08	1 445.6	17.23	19.24	15.01	0.21	5.63
SH2017-4	Chimney	40	5.83	0.24	0.16	8.88	1 220.1	10.26	15.72	15.74	0.03	9.74
SH2017-7	Chimney	50	3.46	0.21	0.36	8.14	1 166.3	10.24	13.06	19.81	0.04	7.32
SH2017-8	Chimney	55	6.03	0.23	0.19	3.79	860.7	12.16	9.68	12.74	0.04	5.76
SH2017-10	Chimney	20	5.10	0.22	0.13	4.67	8 524.5	19.90	15.90	23.88	0.15	25.79
SH2017-2	Block	65	8.22	0.25	0.07	10.56	705.5	7.34	12.89	11.97	0.02	2.21
SH2017-3	Crust	40	5.70	0.31	0.29	5.08	1 344.0	8.57	16.81	17.68	0.03	7.57
SH2017-5	Crust	25	11.74	0.33	0.19	3.74	12 992.8	13.24	32.97	28.01	0.03	9.73
SH2017-6	Crust	50	5.18	0.23	0.16	3.90	2 228.1	22.90	24.47	17.54	0.09	8.14
SH2017-9	Crust	50	5.90	0.25	0.36	3.56	12 038.8	9.89	11.97	22.74	0.12	15.11
SH2017-11	Crust	20	6.81	0.22	0.26	10.72	1 305.1	19.20	18.32	17.23	0.18	5.41
SH2017-12	Crust	60	5.34	0.27	0.05	8.95	19 645.4	35.65	19.09	21.74	0.67	13.85
SH2017-13	Crust	55	0.95	0.28	0.04	3.10	15 116.6	10.20	26.19	23.06	0.04	12.89
SH2017-14	Crust	25	12.99	0.24	0.21	3.20	1 177.7	19.84	20.13	15.16	0.20	5.42
SH2017-15	Crust	30	14.12	0.35	0.11	3.31	4 128.6	6.67	11.59	19.65	0.05	15.40
Haima cold seep												
ROV12	Unknown	10	5.86	0.23	0.33	16.60	939.2	9.89	18.94	23.95	0.04	26.26
ROV2	Unknown	65	0.96	0.23	0.04	12.50	18 237.0	16.52	15.91	95.51	0.24	11.93

activity on its cross section. Samples 12 and 13 contain several bioclasts. Sample 14 that is denser than other samples show no obvious cementation characteristics. Sample 15 that is in a long strip-like shape has several fluid channels in the cross section.

4.2 XRD test result

The XRD analysis shows that the carbonate contents of the samples from Shenhu area are in the range of 20%–65% with an average of 43%. The carbonate content of sample 2 is the highest and that of sample 10 is the lowest (only 20%). The carbonate minerals in the samples are mainly aragonite with different proportions of calcite and dolomite. The carbonate minerals of samples 1–13 are aragonite and calcite, and those of samples 14 and 15 are calcite and dolomite. The clastic quartz content is more than 50% in some samples and that of sample 10 is even as high as 70%. The types of clay minerals are mainly montmorillonite, illite, and chlorite.

The carbonate contents of the two samples from Haima cold seep are significantly different, with that of ROV2 being 65% and ROV12 being 10%. The carbonate minerals are mainly aragonite and calcite, while the quartz content of ROV12 is 85%. The types of clay minerals are mainly kaolinite, chlorite, and illite (Fig.3).

4.3 Main and trace elements

The concentrations of some elements in the samples are listed in Table 1. MgO contents of the 15 samples from Shenhu area vary significantly in the range of 0.95%–14.12%, while higher values are shown on samples 14 and 15, i.e., 12.99% and 14.12%, respectively. Fe contents of all the Shenhu samples are low in the range of 0.14%–0.35%. The highest MnO content in Shenhu samples is 0.36% while the lowest is 0.05%. TiO_2 contents are in the range of 3.08–10.72 μg/g with an average of 5.65 μg/g.

MgO contents of the two samples from Haima cold seep are 5.86% for ROV12 and only 0.96% for ROV2. TiO_2 contents of the samples from Haima cold seep are in the range of 12.50–16.60 μg/g and higher than those of the samples from Shenhu area.

Sr contents of the Shenhu samples vary from 705.5 to 19 645.4 μg/g. In addition, the contents of Ni, Zn, and Ba are very high. Mo and U contents are 0.02–0.67 and 2.21–25.79 μg/g, respectively. U contents of the two samples from Haima cold seep (ROV12 and ROV2), are 26.26 and 11.93 μg/g, while Mo contents are only 0.04 and 0.24 μg/g.

The REE results for the cold-seep carbonate

Table 2 REE results (μg/g), Ce anomalies, and the ratio of Y/Ho of carbonate samples

Sample	La	Ce	Pr	Nd	Sm	Eu	Gd	Tb	Dy	Ho	Er	Tm	Yb	Lu	Y	lg(Ce/Ce*)	Y/Ho
Shenhu area																	
SH2017-1	6.63	15.90	1.82	7.45	1.63	0.31	1.52	0.21	0.59	0.21	0.52	0.07	0.43	0.06	5.92	0.02	28.19
SH2017-4	5.92	14.24	1.61	6.75	1.49	0.29	1.43	0.19	0.63	0.20	0.51	0.07	0.43	0.06	5.69	0.04	28.45
SH2017-7	7.14	17.62	1.95	7.93	1.70	0.33	1.59	0.22	0.63	0.22	0.54	0.08	0.47	0.07	5.86	0.03	26.64
SH2017-8	2.67	6.08	0.73	3.29	0.73	0.14	0.76	0.10	0.31	0.10	0.26	0.04	0.22	0.03	2.94	0.03	29.40
SH2017-10	12.69	29.06	3.10	12.07	2.49	0.48	2.34	0.33	1.02	0.35	0.91	0.13	0.83	0.12	10.71	0.04	30.60
SH2017-2	4.13	10.06	1.11	4.55	0.98	0.19	0.91	0.12	0.36	0.12	0.31	0.04	0.26	0.04	3.43	0.03	28.58
SH2017-3	4.01	9.37	1.06	4.50	1.00	0.20	0.98	0.13	0.44	0.14	0.36	0.05	0.31	0.05	4.19	0.04	29.93
SH2017-5	13.15	31.32	3.25	12.66	2.59	0.50	2.36	0.33	0.91	0.34	0.85	0.12	0.74	0.10	9.70	0.04	28.53
SH2017-6	14.13	31.38	3.62	14.51	3.24	0.66	3.24	0.45	1.73	0.49	1.26	0.18	1.12	0.16	15.18	0	30.98
SH2017-9	8.10	20.75	2.08	8.10	1.74	0.34	1.65	0.24	0.85	0.26	0.67	0.10	0.63	0.09	7.62	0.06	29.31
SH2017-11	5.77	12.97	1.57	6.56	1.44	0.29	1.39	0.19	0.62	0.20	0.50	0.07	0.42	0.06	5.93	-0.01	29.65
SH2017-12	10.28	22.40	2.51	9.98	2.01	0.38	1.83	0.25	0.70	0.27	0.70	0.10	0.61	0.09	8.19	0.01	30.33
SH2017-13	10.80	22.98	2.45	9.47	1.77	0.33	1.54	0.21	0.45	0.22	0.57	0.08	0.50	0.07	6.71	0.02	30.50
SH2017-14	6.24	13.40	1.68	6.95	1.50	0.29	1.42	0.19	0.54	0.19	0.48	0.07	0.40	0.06	5.49	-0.01	28.89
SH2017-15	10.77	27.17	2.77	10.83	2.38	0.47	2.35	0.34	1.27	0.37	0.98	0.14	0.91	0.13	11.02	0.06	29.78
Haima cold seep																	
ROV12	3.14	7.99	0.91	4.11	0.98	0.23	1.09	0.14	0.59	0.15	0.38	0.05	0.31	0.03	4.25	0.02	28.33
ROV2	6.45	10.83	1.44	5.90	1.23	0.28	1.24	0.17	0.63	0.19	0.51	0.07	0.44	0.07	6.54	-0.07	34.42

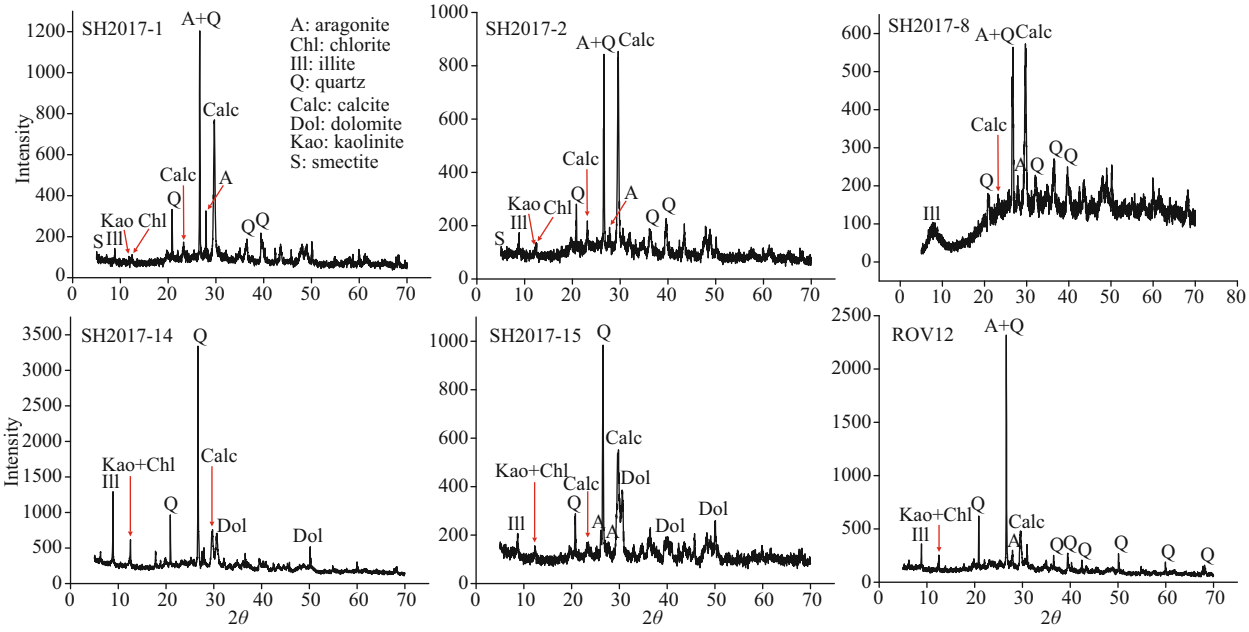

Fig.3 Representative XRD analysis results of cold-seep carbonate samples

The carbonate content of our samples ranges 20%-65% on average of 43%, and aragonite plays the main role in most of samples.

samples are depicted in Table 2. To define the REE sources of our samples, we standardized the REE values based on Post-Archean Australian Shale (PAAS, McLennan, 1989) and created the REE distribution curves (Fig.4).

The REE contents of the Shenhu carbonates vary dramatically in the range of 15.46–76.17 μg/g with an average of 43.98 μg/g. The La_N/Sm_N and Yb_N/Sm_N values of the samples are in the range of 0.53–0.89 (mean value of 0.65) and 0.52–0.75 (mean value

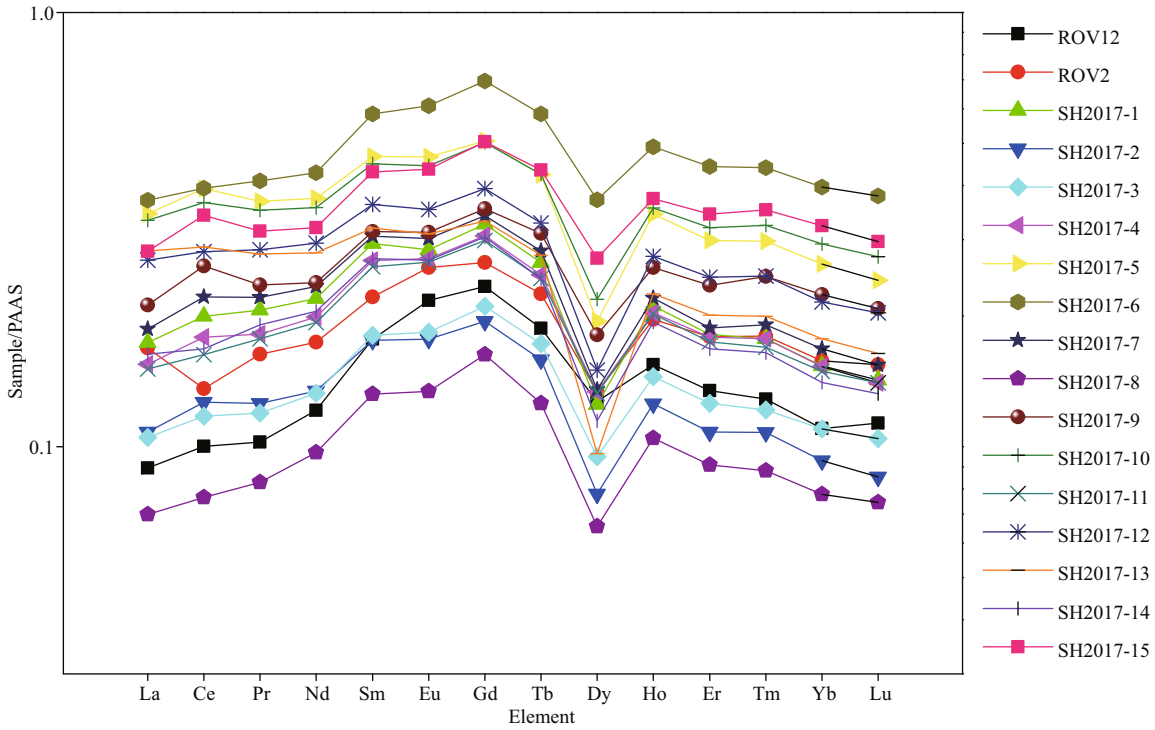

Fig.4 REE distribution curves after PAAS standardization (McLennan, 1989)

A similar feature rich in the middle rare earth elements (MREEs) is present in our samples.

Table 3 Carbon and oxygen isotopic compositions of carbonate samples

Sample	$\delta^{13}C$ (‰ VPDB)	$\delta^{18}O$ (‰ VPDB)
Shenhu area		
SH2017-1	-34.25	2.09
SH2017-4	-33.72	2.53
SH2017-7	-34.07	2.36
SH2017-8	-22.34	2.05
SH2017-10	-49.80	2.66
SH2017-2	-27.70	2.84
SH2017-3	-39.81	2.26
SH2017-5	-56.25	2.76
SH2017-6	-50.65	3.46
SH2017-9	-53.35	3.23
SH2017-11	-30.55	2.41
SH2017-12	-59.30	3.09
SH2017-13	-51.45	2.44
SH2017-14	-32.62	3.23
SH2017-15	-47.96	3.90
Haima cold seep		
ROV12	-37.28	2.79
ROV2	-37.91	3.76

of 0.60), respectively. These values are lower than the respective ratios for modern seawater (La_N/Sm_N=0.57–1.37, Yb_N/Sm_N=3.31–6.47) (Alibert, 2016). The Y/Ho ratios of the Shenhu samples are in the range of 26.64–30.98 with an average of 29.32.

The total REE contents of the Haima samples are lower than those of the Shenhu samples. The La_N/Sm_N and Yb_N/Sm_N ratios of the Haima samples are 0.51–0.76 (mean value of 0.63) and 0.62–0.71 (mean value of 0.66), respectively, which are similar to those of the Shenhu samples. The Y/Ho ratios of the Haima samples are in the range of 28.33–34.42 with an average of 31.38.

4.4 Carbon and oxygen isotopic composition

The carbon and oxygen isotopic compositions of all the samples are shown in Table 3. The Shenhu samples have relatively negative carbon isotopic composition. The values of $\delta^{13}C$ vary from -22.34‰ to -59.30‰ VPDB with an average of -41.59‰ VPDB. The difference between the $\delta^{13}C$ values of the two Haima samples is insignificant (-37.91‰ VPDB for the ROV2 and -37.91‰ VPDB for ROV12).

The oxygen isotopic compositions of the Shenhu samples in the range of 2.05‰–3.90‰ and with an average value of 2.75‰, are obviously heavier than that of seawater. The $\delta^{18}O$ values of the Haima

samples show obvious enrichment, and the $\delta^{18}O$ value of ROV2 is as high as 3.76‰.

5 DISCUSSION

5.1 Possible factors affecting morphology

Cold-seep carbonates in the SCS occur in the form of blocks, chimneys, branches, columns, and biochemical reefs (Han et al., 2008; Tong et al., 2013; Feng et al., 2018). Researches have shown that both internal and external factors influence the formation of cold-seep carbonates (Mazzini et al., 2006; Magalhães et al., 2012). Internal factors include the composition and flow rate of fluid in cold-seep seepage and biological activities (Mazzini et al., 2006; Suess, 2014), while external factors include regional tectonics, chemical properties of bottom water, and local erosion (Schlüter et al., 1998; Borowski et al., 1999; Stakes et al., 1999; Díaz-del-Río et al., 2003; Mazzini et al., 2006; Suess, 2014). In this study, the carbonates from Shenhu area were procured from the same site, and there was little difference among the samples in terms of bottom water, regional geology or other external factors. Therefore, it is speculated that mainly internal factors affected the occurrence of the samples. Generally, the block form and dense texture indicate a strong compaction and deep formation depth; chimney shape may inherit from fluid channels, which reflects significant pipeline development and is usually associated with hydrocarbon-rich fluid migration through vertical fractures or hydrocarbon fluid saturation in the pores of submarine sediments (Díaz-del-Río et al., 2003; Ge et al., 2010; Nyman et al., 2010; Feng et al., 2018); crust form may appears in the shallow depth close to the seafloor, possibly suffering the erosion of undercurrent (Magalhães et al., 2012). In samples 1 and 4, the obvious biological features indicate the medium-high flux of seepage fluid. Dense texture of sample 2 is not conducive to fluid migration, reflecting a greater compaction, and sample 2 could have precipitated at deeper depth during a lower flux. Evident channels shown in our samples present a relatively focused fluid migration (Fig.2, samples 7 and 8). The quality and quantity of holes observed in the samples may be the indicator of either difference in the strength of fluid leakage or biological activity, and higher porosity generally provides a better fluid migration environment with less compaction (Fig.2).

5.2 Sedimentary environment of cold-seep carbonates

The mineralogy of cold-seep carbonates can well reflect the sedimentary environment (Greinert et al., 2001; Naehr et al., 2007). The presence of SO_4^{2-} in pore water shows stronger inhibition effect on the precipitation of calcite and dolomite than on that of aragonite (Aloisi et al., 2000). Therefore, aragonite usually precipitate in the shallower SMTZ, while calcite and dolomite tend to form more deeply (Paull and Ussler III, 2008; Gong et al., 2018). The Sr content in our samples from both Shenhu area and Haima cold seep is significantly higher than that of common marine carbonates (610 μg/g), of which low magnesium calcite is usually dominated carbonate facies (Turekian and Wedepohl, 1961). The Sr content of cold-seep carbonates is related to their mineralogy, and Ca^{2+} in aragonite is preferentially replaced by Sr^{2+}. Therefore, the content of Sr in aragonite is significantly higher than that in calcite (Peckmann et al., 2001), which is consistent with the results of XRD analysis. Furthermore, the content of aragonite in cold-seep carbonates with Sr content greater than 104 μg/g is relatively high, which results from a shallower formation depth influenced by the active cold-seep activity. The distinct proportion of calcite in samples 2, 7, and 8 indicates the relatively high deposition depth and low cold-seep fluid flow (Fig.2). Specially, a certain proportion of dolomite appears in samples 14 and 15. Though the precipitation mechanism of dolomite remains mysterious, it generally tends to precipitate under the conditions of high alkalinity, low sulfate concentration and strong biological activities (Warren, 2000; Tong et al., 2012; Lu et al., 2018). Zhang et al. (2012) suggested that it was not the consumption of sulfate but presence of dissolved sulfide that promotes the dehydration of Mg^{2+}, which is more conducive to the formation of dolomite under the condition of strongly reduced sulfide. Magalhães et al. (2012) believed the formation of dolomite is related to the erosion of undercurrent. Both samples 14 and 15 show a relatively high MgO content, which may induce the formation of dolomite. However, different occurrences appear in samples 14 and 15: high porosity and distinct fluid migration traces in sample 15 while low porosity and dense texture in sample 14. More diffuse seepage features in sample 15 may be strongly associated with the methane and sulphate gradients and may form during cementation of subsurface permeable layers. It indicates the strong microbial activity in sample 15 as

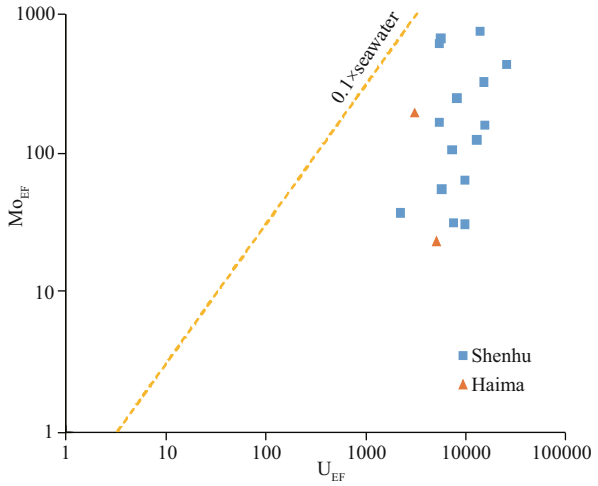

Fig.5 Enrichment factors (EF); Mo_{EF} vs. U_{EF} for cold-seep carbonates in this study modified from Algeo and Tribovillard (2009)

Mo_{EF}/U_{EF} of seawater=3.1. The Mo_{EF}/U_{EF} ratios are less than 0.1 times corresponding value of seawater.

well. Sample 14 may precipitate in the deeper depth and be exposed to the seafloor due to the heavy erosion of undercurrent.

Additionally, the low carbonate contents of samples 5, 10, 11, 14, and 15 with the relatively high contents of quartz emphasize the great effect of terrestrial sediments and deeper formation depth in lower flux seepage. Similarly, clay minerals, which are around 10% in content, may also influence the formation of carbonates.

The carbonates of the Haima cold seep contain significantly higher content of aragonite, suggesting the shallower precipitation depth and stronger cold-seep activity than that of Shenhu area. Significant influence of terrestrial deposition also imprinted in Haima samples as the low carbonate content of ROV12 and the certain contain of clay minerals are shown.

In recent years, the enrichment factors of trace elements, especially Mo and U, have been commonly used to trace the redox condition during the formation of cold-seep carbonate (Algeo and Tribovillard, 2009; Palomares et al., 2012; Sato et al., 2012; Tribovillard et al., 2012; Hu et al., 2015). Although there are small deposits of both U and Mo in the ocean, U is dissolved in water in the high state as $UO_2(CO_3)_3^{4-}$ with a residence time of up to 450 ka in oxidized seawater, while Mo exists in seawater as MoO_4^{2-} with a residence time of up to 780 ka (Algeo and Tribovillard, 2009; Hu et al., 2015). Under the anoxic condition without free H_2S in the water column, U (VI) is reduced to UO_2 during precipitation at the redox boundary of Fe (II–III), while Mo needs to be deposited at sedimentary depths where H_2S is present (Zheng et al., 2002; Piper and Calvert, 2009; Chen et al., 2016; Smrzka et al., 2020). Hence, the deposition of U takes priority over that of Mo, resulting in U_{EF}>Mo_{EF}. Mo and U are significantly enriched in our samples from both regions, which indicates the anoxic formation environments and an overlap or at least a close proximity of the iron reduction zone and the SMTZ in the active cold seep (Chen et al., 2016; Lin et al., 2021) (Fig.5).

The REE composition is often used to determine the redox conditions and trace the fluid properties during carbonate formation (Haley et al., 2004; Chen et al., 2005; Himmler et al., 2010; Bayon et al., 2011; Rongemaille et al., 2011; Han et al., 2014). The REE composition of carbonates is usually strongly influenced by the surrounding seawater and pore water. The similar patterns of REE distribution standardized by PAAS among all the samples are interpreted as a consistent sedimentary fluid environment (Fig.4). REE distribution patterns of the samples have typical features of that of anoxic pore water with an middle rare earth element (MREE) enrichment pattern, illustrating that the carbonates may have precipitated from the pore water. Previous studies have shown that the REE distribution patterns of pore water are related to depth and that the MREE enrichment pattern generally appears in the reduction zone of iron (Haley et al., 2004; Kim et al., 2012), revealing the anoxic precipitation environment of the carbonates.

The Y/Ho ratio is useful for distinguishing among different types of water and their respective sediments (Nothdurft et al., 2004). Jakubowicz et al. (2015) suggested that owing to the interaction with bedrocks and sediments, typical seepage fluids (without any influence of seawater) have a low Y/Ho value, which may be close to those of the upper continental crust (27.5) and chondrite (25–28) (Taylor and McLennan, 1985; Kamber et al., 2005). Seawater usually shows a high Y/Ho value of 60–150 (Nozaki et al., 1997; Lawrence and Kamber, 2006). The Y/Ho values of the Shenhu area and Haima samples are similar, ranging from 26.64 to 34.42. These values are slightly higher than the Y/Ho value of typical seepage fluid and significantly lower than that of seawater, suggesting that the samples were less affected by seawater.

Ce anomaly is usually used to clarify the sedimentary environments of cold-seep carbonates. A

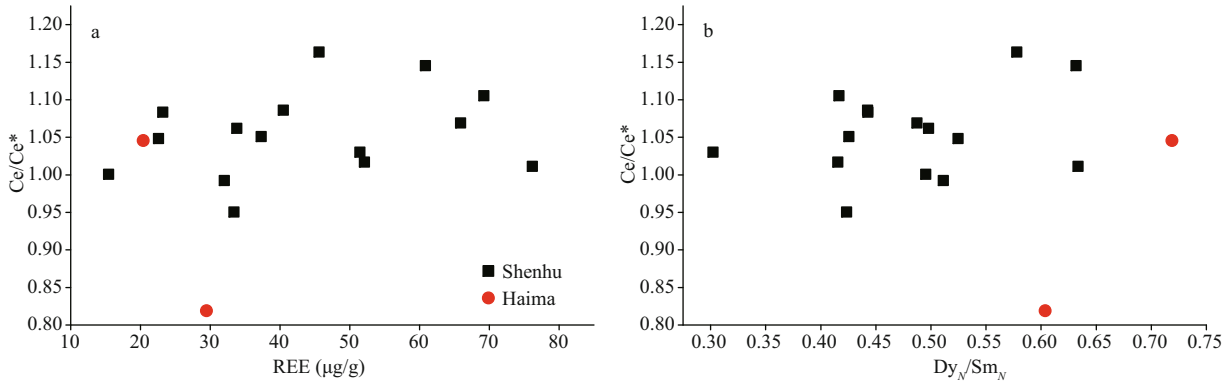

Fig.6 Cross-plots of various parameters calculated from the PAAS-normalized REE

a. REE vs. Ce/Ce*; b. Dy_N/Sm_N vs. Ce/Ce*. No correlation is shown in both figures, so our results of Ce/Ce* reflect the original Ce anomaly of the samples.

negative Ce anomaly after PAAS standardization usually indicates an oxidation environment, while an absent or positive Ce anomaly indicates a reduction environment. Previous studies have shown that late diagenesis may change the main Ce/Ce* values of carbonates (Feng et al., 2009; Hu et al., 2014), leading to a positive correlation between Ce/Ce* and REE, and a negative correlation between Ce/Ce* and Dy_N/Sm_N (Shields and Stille, 2001). We can see from Fig.6 that Ce/Ce* has no correlation with REE or Dy_N/Sm_N, so the results of Ce/Ce* reflect the original Ce anomaly and can indicate the original sedimentary environment of the samples. Traditionally, cold-seep carbonates are supposed to precipitate in a reductive environment, with no or positive Ce anomaly. However, in recent years, studies on cold-seep carbonates in Mexico, Black Sea, Congo, and other places have shown negative Ce anomalies, indicating aerobic environments (Feng et al., 2009; Ge et al., 2010; Tong et al., 2012). It is speculated that the cold seep may have had a temporary aerobic environment, which may be related to the change in fluid leakage rate (Feng et al., 2009, 2010; Birgel et al., 2011; Tong et al., 2012). The lg(Ce/Ce*) values of the Shenhu samples range from -0.01 to 0.06, most suggesting no or positive Ce anomaly. Samples 11 and 14 show a slightly negative Ce anomaly. The formation environments of samples 9 and 15 may have been slightly more reductive than those of the other samples because they show true positive Ce anomaly. Sample ROV12 shows no Ce anomaly while Sample ROV2 shows an obviously negative Ce anomaly, indicating that the latter might have experienced a temporary oxidation environment or may have been mixed with seawater with negative Ce negative anomaly (Hu et al., 2014) (Fig.7).

As mentioned above, all samples present more

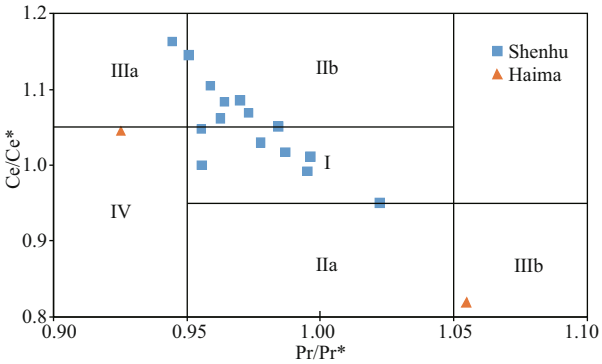

Fig.7 Ce/Ce* vs. Pr/Pr* (Bau and Dulski, 1996; Shields and Webb, 2004)

Field I: neither Ce nor La anomaly; field IIa: positive La anomaly, no Ce anomaly; field IIb: negative La anomaly, no Ce anomaly; field IIIa: positive Ce anomaly; field IIIb: negative Ce anomaly; field IV: La anomaly, no Ce anomaly.

than one type carbonate mineral phases and different redox condition features (e.g. lg(Ce/Ce*) and Fig.7), possibly indicating multi-stage formation. Feng et al. (2018) concluded that several regional factors including temporal and spatial variation of cold-seep fluid flow would generate the heterogeneity in the facies of seep carbonates. Here, we have ventured to speculate that the aragonite-dominated carbonates are formed close to the seafloor and the lower seepage flux would induce the precipitation of dense carbonate with a higher proportion of calcite (samples 2, 7, and 8). Low carbonate content along with high debris content and main carbonate phases (calcite and dolomite) in samples 14 and 15 indicate a deeper formation depth in a low fluid seepage and a relatively complex formation mechanism possibly induced by high Mg content and strong microbial activity.

Although the information of the Haima samples is limited, we can infer from their geochemical characteristics that their precipitation is influenced by

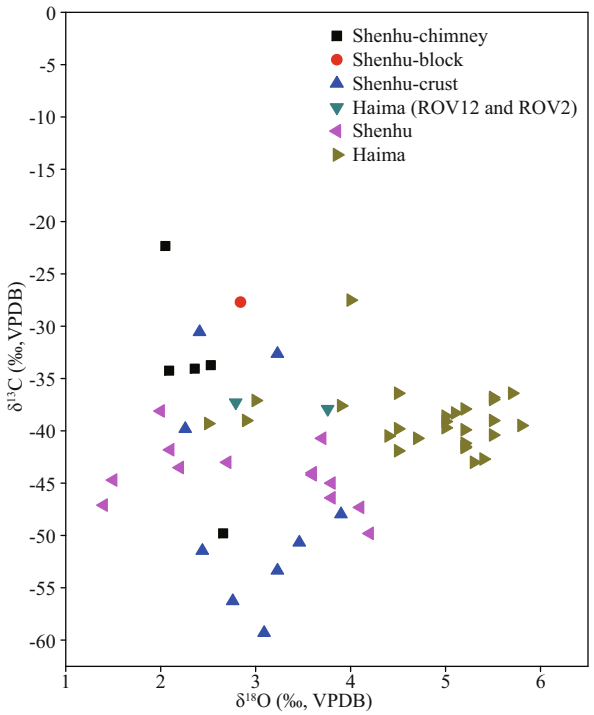

Fig.8 $\delta^{13}C$ and $\delta^{18}O$ values of cold-seep carbonates

Data named Shenhu area and Haima cold seep come from previous studies (Tong et al., 2013; Liang et al., 2017). Other data are from the results in this study.

both seawater and seepage fluids and may have experienced a short-term oxidized environment.

5.3 $\delta^{13}C$ and $\delta^{18}O$ analysis for source of cold-seep fluid

Cold-seep carbonates generally inherit the carbon isotopic composition of the cold-seep fluid via AOM. Hence, this characteristic of the sample can be used to determine the source of carbon, and its variation reflects the mixing degree of different carbon sources (Suess, 2014; Feng et al., 2018). Several studies on the carbon oxygen isotopes of cold-seep carbonates have been conducted in Shenhu area and Haima cold seep (Feng et al., 2018). Our Shenhu samples have a relatively negative carbon isotopic composition with an average value of -41.59‰, consistent with the result of previous studies (Feng et al., 2018; Fig.8), which is lighter than those of normal marine carbonates ($\delta^{13}C$ ranging from -3‰ to 3‰ VPDB; Anderson and Arthur, 1983), indicating a degree of AOM function and mixed methane source between biogenic and thermogenic methane (Ge et al., 2011; Zhang et al., 2017). Additionally, $\delta^{13}C$ of our samples varies widely, and most of crust carbonates except for samples 3, 11, and 14 presents more depleted ^{13}C than that of the other two shape types. As discussed above, morphology is correlated firmly with the formation environment, and the deeper where carbonate formed may spark a stronger effect of thermogenic methane with higher $\delta^{13}C$. Other factors such as the permeable condition in the sediment, heterogeneity of methane properties and seawater will also influence $\delta^{13}C$ of carbonates.

The $\delta^{13}C$ values of the two Haima cold-seep carbonates, i.e., ROV2 and ROV12, are similar to those of previous studies (Fig.8), identifying a mostly biogenic origin of methane (Liang et al., 2017; Guan et al., 2018). Considering that the only 10% carbonate content of ROV12 implies significant influence of background deposition, the addition of seawater may lead to the bias of ^{13}C during its precipitation.

The oxygen isotopic compositions of the cold-seep carbonates are generally close to that of seawater and mainly affected by the formation temperature, the mineral composition, and $\delta^{18}O$ of pore water (Aloisi et al., 2000). The oxygen isotopes of the samples from both Shenhu area and Haima cold seep are obviously heavier than that of seawater. The reason for ^{18}O enrichment may be that ^{18}O-rich fluids participate in the precipitation of cold-seep carbonates. The main sources of ^{18}O-rich fluids are the dissociation of gas hydrates and dehydration of clay minerals (Feng and Chen, 2015; Liang et al., 2017; Feng et al., 2018). Gas hydrate dissociation has been detected in the Shenhu area (Suess, 2005; Zhang et al., 2007, 2019). Studies on the genesis of gas hydrates in the Shenhu area show that the source of gas hydrates is a mixture of thermogenic and microbial gases, and the value of $\delta^{13}C$ of gas from the dissociation of hydrates is between -40‰ and -60‰ (Zhang et al., 2017), which does not conflict with our results of C isotope and has sufficient potential as a source of methane in the study area. Hence, water from hydrate dissociation may participate in the precipitation, increasing the $\delta^{18}O$ value of the cold-seep carbonates (Feng et al., 2018).

A high ^{18}O may also reflect a local low-temperature area, while a relatively low ^{18}O may reflect a local high-heat flow (Feng and Chen, 2015; Liang et al., 2017; Yang et al., 2018). The dissociation of hydrates and the possible dehydration of clay minerals in this area affect the enrichment of ^{18}O in carbonates by ore-forming fluids, thus leading to the illusion of lower temperature. The age of the Shenhu samples in this study is unknown and hence, the specific temperature of the formation of the cold-seep carbonates cannot be determined. Therefore, the contribution of formation temperature and methane-rich fluid to the ^{18}O values of the cold-seep carbonates in this area

requires further study.

The samples from the Haima cold-seep area were collected at a temperature of approximately 3 °C from the bottom of the sea, and the ^{14}C dating results are in the range of 5.1–6.1 ka and 2.9–3.9 ka (Liang et al., 2017). Many studies have shown that the sea level of the SCS had remained relatively stable over the past 6 000 years, with no significant change in the sea surface temperature (Pelejero et al., 1999; Zhao et al., 2006; Steinke et al., 2011). Therefore, we use the temperature of underlying water as the reference value of diagenetic temperature. It was assumed that the samples were formed from the current bottom water at a temperature of 3.0 °C and $\delta^{18}O$ value of 0‰ VSMOW. The oxygen isotopic composition was calculated using Eq.3 when aragonite is in equilibrium with seawater. The oxygen isotopic composition at equilibrium between calcite and seawater was calculated using Eq.4. The conversion Eq.5 between $\delta^{18}O_{VPDB}$ and $\delta^{18}O_{VSMOW}$ was carried out using the equation proposed by Coplen et al. (1983). The definition of the oxygen isotopic fractionation factor, α, is given by Eq.6.

$$10^3\ln\alpha_{aragonite\text{-}water}=17.88\times10^3/T-31.14 \quad \text{(Kim et al., 2007)}, \quad (3)$$

$$10^3\ln\alpha_{calcite\text{-}water}=18.03\times10^3/T-32.4 \quad \text{(Kim and O'Neil, 1997)}, \quad (4)$$

$$\delta^{18}O_{(VSMOW)}=1.03091\times\delta^{18}O_{(VPDB)}+30.91 \quad \text{(Coplen et al., 1983)}, \quad (5)$$

$$\alpha_{aragonite/calcite\text{-}water}=(1000+\delta^{18}O_{aragonite/calcite})/(1000+\delta^{18}O_{water}). \quad (6)$$

Here, T is the absolute temperature of seawater (K), $\delta^{18}O_{aragonite/calcite}$ in Eq.6 and $\delta^{18}O_{water}$ used here are given in the δ-notation (‰) relative to the VSMOW standard.

The oxygen isotopic compositions of aragonite and calcite at equilibrium with seawater were 3.2‰ VPDB and 2.5‰ VPDB, respectively, which were lower than the measured $\delta^{18}O$ values of the Haima samples, which further confirms that ^{18}O-rich fluid was involved in the precipitation. The source of biogenic methane indicates that they originated from the shallow strata, and the temperature and pressure conditions in the source area could not facilitate the transformation from montmorillonite to illite. In addition, gas hydrate has been recovered by the gravity and piston core from the cold seep (Liang et al., 2017). Therefore, we speculated that the source of ^{18}O-rich fluid here was mainly the dissociation of hydrates in the shallow strata.

6 CONCLUSION

Morphology and mineralogy of the studied cold-seep carbonates from Shenhu area reflect the different environment of formation and fluid migration. Enrichment of U and Mo and REE features (including MREE enrichment, absent or slightly positive Ce anomaly) in the samples indicate the anoxic precipitation environment. And some samples may experience a periodical oxidation or influence by seawater, showing the negative Ce anomalies. Compared with the samples from the two areas, we conclude that the formation depths of the Haima samples were shallower and represent a stronger cold-seep activity.

Cold-seep carbonates from both Shenhu area and Haima cold seep are methane-derived, while the former mainly originate from a mixture of thermogenic and microbial gases, and the latter from biogenic gas. The ^{18}O-rich fluid was mainly from the dissociation water of gas hydrates.

Our study makes the comparison between Shenhu area and Haima cold seep to get better understanding of the cold seep system in SCS and is conductive to the exploration of gas hydrate. However, lack of analyses such as microphase observation by scanning electron microscope due to loose samples, and limited data restrict our further analysis. Hence, more samples and comprehensive studies will be needed in the future.

7 DATA AVAILABILITY STATEMENT

The data that support the findings of this study are available from the corresponding authors upon reasonable request.

8 ACKNOWLEDGMENT

We are grateful to the two anonymous reviewers for the valuable suggestions.

References

Algeo T J, Tribovillard N. 2009. Environmental analysis of paleoceanographic systems based on molybdenum-uranium covariation. *Chemical Geology*, **268**(3-4): 211-225, https://doi.org/10.1016/j.chemgeo.2009.09.001.

Alibert C. 2016. Rare earth elements in Hamersley BIF minerals. *Geochimica et Cosmochimica Acta*, **184**: 311-328, https://doi.org/10.1016/j.gca.2016.03.026.

Aloisi G, Pierre C, Rouchy J M, Foucher J P, Woodside J, the MEDINAUT Scientific Party. 2000. Methane-related authigenic carbonates of eastern Mediterranean Sea mud

volcanoes and their possible relation to gas hydrate destabilisation. *Earth and Planetary Science Letters*, **184**(1): 321-338, https://doi.org/10.1016/S0012-821X(00)00322-8.

Anderson T F, Arthur M A. 1983. Stable isotopes of oxygen and carbon and their application to sedimentologic and paleoenvironmental problems. *In*: Arthur M A eds. Stable Isotopes in Sedimentary Geology. Society of Economic Paleontologists and Mineralogists, Tulsa, Oklahoma. p.1-151.

Bau M, Dulski P. 1996. Distribution of yttrium and rare-earth elements in the Penge and Kuruman iron-formations, Transvaal Supergroup, South Africa. *Precambrian Research*, **79**(1-2): 37-55, https://doi.org/10.1016/0301-9268(95)00087-9.

Bayon G, Birot D, Ruffine L, Caprais J C, Ponzevera E, Bollinger C, Donval J P, Charlou J L, Voisset M, Grimaud S. 2011. Evidence for intense REE scavenging at cold seeps from the Niger Delta margin. *Earth and Planetary Science Letters*, **312**(3-4): 443-452, https://doi.org/10.1016/j.epsl.2011.10.008.

Birgel D, Feng D, Roberts H, Peckmann J. 2011. Changing redox conditions at cold seeps as revealed by authigenic carbonates from Alaminos Canyon, northern Gulf of Mexico. *Chemical Geology*, **285**(1-4): 82-96, https://doi.org/10.1016/j.chemgeo.2011.03.004.

Boetius A, Wenzhöfer F. 2013. Seafloor oxygen consumption fuelled by methane from cold seeps. *Nature Geoscience*, **6**(9): 725-734, https://doi.org/10.1038/ngeo1926.

Borowski W S, Paull C K, Ussler III W. 1999. Global and local variations of interstitial sulfate gradients in deep-water, continental margin sediments: sensitivity to underlying methane and gas hydrates. *Marine Geology*, **159**(1-4): 131-154, https://doi.org/10.1016/S0025-3227(99)00004-3.

Campbell K A. 2006. Hydrocarbon seep and hydrothermal vent paleoenvironments and paleontology: past developments and future research directions. *Palaeogeography*, *Palaeoclimatology*, *Palaeoecology*, **232**(2-4): 362-407, https://doi.org/10.1016/j.palaeo.2005.06.018.

Chen D F, Cathles L M. 2005. On the thermal impact of gas venting and hydrate crystallization. *Journal of Geophysical Research*: *Solid Earth*, **110**(B11): B11204, https://doi.org/10.1029/2004JB003533.

Chen D F, Huang Y Y, Yuan X L, Cathles L M. 2005. Seep carbonates and preserved methane oxidizing archaea and sulfate reducing bacteria fossils suggest recent gas venting on the seafloor in the Northeastern South China Sea. *Marine and Petroleum Geology*, **22**(5): 613-621, https://doi.org/10.1016/j.marpetgeo.2005.05.002.

Chen F, Hu Y, Feng D, Zhang X, Cheng S H, Cao J, Lu H F, Chen D F. 2016. Evidence of intense methane seepages from molybdenum enrichments in gas hydrate-bearing sediments of the northern South China Sea. *Chemical Geology*, **443**: 173-181, https://doi.org/10.1016/j.chemgeo.2016.09.029.

Chen H, Wang S H, Chen Z, Yan W, Li G. 2015. Geochemical and magnetic signals for the mud volcano-induced methane seepage in the core sediments of Shenhu area, northern South China Sea. *Environmental Earth Sciences*, **73**(10): 6365-6378, https://doi.org/10.1007/s12665-014-3860-y.

Coplen T B, Kendall C, Hopple J. 1983. Comparison of stable isotope reference samples. *Nature*, **302**(5905): 236-238, https://doi.org/10.1038/302236a0.

Díaz-del-Río V, Somoza L, Martínez-Frias J, Mata M P, Delgado A, Hernandez-Molina F J, Lunar R, Martín-Rubí J A, Maestro A, Fernández-Puga M C, León R, Llave E, Medialdea T, Vázquez J T. 2003. Vast fields of hydrocarbon-derived carbonate chimneys related to the accretionary wedge/olistostrome of the Gulf of Cádiz. *Marine Geology*, **195**(1-4): 177-200, https://doi.org/10.1016/S0025-3227(02)00687-4.

Feng D, Chen D F, Peckmann J, Bohrmann G. 2010. Authigenic carbonates from methane seeps of the northern Congo fan: microbial formation mechanism. *Marine and Petroleum Geology*, **27**(4): 748-756, https://doi.org/10.1016/j.marpetgeo.2009.08.006.

Feng D, Chen D F, Peckmann J. 2009. Rare earth elements in seep carbonates as tracers of variable redox conditions at ancient hydrocarbon seeps. *Terra Nova*, **21**(1): 49-56, https://doi.org/10.1111/j.1365-3121.2008.00855.x.

Feng D, Chen D F. 2015. Authigenic carbonates from an active cold seep of the northern South China Sea: new insights into fluid sources and past seepage activity. *Deep Sea Research Part II*: *Topical Studies in Oceanography*, **122**: 74-83, https://doi.org/10.1016/j.dsr2.2015.02.003.

Feng D, Qiu J W, Hu Y, Peckmann J, Guan H X, Tong H P, Chen C, Chen J X, Gong S G, Li N, Chen D F. 2018. Cold seep systems in the South China Sea: an overview. *Journal of Asian Earth Sciences*, **168**: 3-16, https://doi.org/10.1016/j.jseaes.2018.09.021.

Ge L, Jiang S Y, Swennen R, Yang T, Yang J H, Wu N Y, Liu J, Chen D H. 2010. Chemical environment of cold seep carbonate formation on the northern continental slope of South China Sea: evidence from trace and rare earth element geochemistry. *Marine Geology*, **277**(1-4): 21-30, https://doi.org/10.1016/j.margeo.2010.08.008.

Ge L, Jiang S Y, Yang T, Yang J H, Wu N Y, Zhang G X, Liu J. 2011. Glycerol ether biomarkers and their carbon isotopic compositions in a cold seep carbonate chimney from the Shenhu area, northern South China Sea. *Chinese Science Bulletin*, **56**(16): 1700-1707, https://doi.org/10.1007/s11434-011-4486-z.

Gong S G, Hu Y, Li N, Feng D, Liang Q Y, Tong H P, Peng Y B, Tao J, Chen D F. 2018. Environmental controls on sulfur isotopic compositions of sulfide minerals in seep carbonates from the South China Sea. *Journal of Asian Earth Sciences*, **168**: 96-105, https://doi.org/10.1016/j.jseaes.2018.04.037.

Gong Z S, Li S T, Xie T. 1997. Continental Margin Basin Analysis and Hydrocarbon Accumulation of the Northern South China Sea. Science Press, Beijing. p.443-498. (in Chinese)

Greinert J, Bohrmann G, Suess E. 2001. Gas hydrate-associated

carbonates and methane-venting at Hydrate Ridge: classification, distribution, and origin of authigenic lithologies. *In*: Natural Gas Hydrates: Occurrence, Distribution, and Detection: Occurrence, Distribution, and Detection. American Geophysical Union, Washington. p.131-143, https://doi.org/10.1029/GM124p0099.

Guan H X, Birgel D, Peckmann J, Liang Q Y, Feng D, Yang S X, Liang J Q, Tao J, Wu N Y, Chen D F. 2018. Lipid biomarker patterns of authigenic carbonates reveal fluid composition and seepage intensity at Haima cold seeps, South China Sea. *Journal of Asian Earth Sciences*, **168**: 163-172, https://doi.org/10.1016/j.jseaes.2018.04.035.

Haley B A, Klinkhammer G P, McManus J. 2004. Rare earth elements in pore waters of marine sediments. *Geochimica et Cosmochimica Acta*, **68**(6): 1265-1279, https://doi.org/10.1016/j.gca.2003.09.012.

Han X Q, Suess E, Huang Y Y, Wu N Y, Bohrmann G, Su X, Eisenhauer A, Rehder G, Fang Y X. 2008. Jiulong methane reef: microbial mediation of seep carbonates in the South China Sea. *Marine Geology*, **249**(3-4): 243-256, https://doi.org/10.1016/j.margeo.2007.11.012.

Han X Q, Suess E, Liebetrau V, Eisenhauer A, Huang Y Y. 2014. Past methane release events and environmental conditions at the upper continental slope of the South China Sea: constraints by seep carbonates. *International Journal of Earth Sciences*, **103**(7): 1873-1887, https://doi.org/10.1007/s00531-014-1018-5.

Han X Q, Yang K H, Huang Y Y. 2013. Origin and nature of cold seep in northeastern Dongsha area, South China Sea: evidence from chimney-like seep carbonates. *Chinese Science Bulletin*, **58**(30): 3689-3697, https://doi.org/10.1007/s11434-013-5819-x.

He J X, Chen S H, Liu H L, Liu S L. 2009. Natural gas genetic types and source rocks in the northern slope of Baiyun Sag to Panyu Low Uplift in Pearl River Mouth Basin. *Acta Petrolei Sinica*, **30**(1): 16-21, https://doi.org/10.7623/syxb200901004. (in Chinese with English abstract)

Himmler T, Bach W, Bohrmann G, Peckmann J. 2010. Rare earth elements in authigenic methane-seep carbonates as tracers for fluid composition during early diagenesis. *Chemical Geology*, **277**(1-2): 126-136, https://doi.org/10.1016/j.chemgeo.2010.07.015.

Hu Y, Feng D, Liang Q Y, Xia Z, Chen L Y, Chen D F. 2015. Impact of anaerobic oxidation of methane on the geochemical cycle of redox-sensitive elements at cold-seep sites of the northern South China Sea. *Deep Sea Research Part II*: *Topical Studies in Oceanography*, **122**: 84-94, https://doi.org/10.1016/j.dsr2.2015.06.012.

Hu Y, Feng D, Peckmann J, Roberts H H, Chen D F. 2014. New insights into cerium anomalies and mechanisms of trace metal enrichment in authigenic carbonate from hydrocarbon seeps. *Chemical Geology*, **381**: 55-66, https://doi.org/10.1016/j.chemgeo.2014.05.014.

Hui G G, Li S Z, Guo L L, Zhang G X, Gong Y H, Somerville I D, Zhang Y, Zheng Q L, Zang Y B. 2016. Source and accumulation of gas hydrate in the northern margin of the South China Sea. *Marine and Petroleum Geology*, **69**: 127-145, https://doi.org/10.1016/j.marpetgeo.2015.10.009.

Jakubowicz M, Dopieralska J, Belka Z. 2015. Tracing the composition and origin of fluids at an ancient hydrocarbon seep (Hollard Mound, Middle Devonian, Morocco): a Nd, REE and stable isotope study. *Geochimica et Cosmochimica Acta*, **156**: 50-74, https://doi.org/10.1016/j.gca.2015.02.027.

Joseph A. 2017. Seafloor hot chimneys and cold seeps: mysterious life around them. *In*: Joseph A ed. Investigating Seafloors and Oceans. Elsevier, Amsterdam. p.307-375, https://doi.org/10.1016/B978-0-12-809357-3.00006-0.

Kamber B S, Greig A, Collerson K D. 2005. A new estimate for the composition of weathered young upper continental crust from alluvial sediments, Queensland, Australia. *Geochimica et Cosmochimica Acta*, **69**(4): 1041-1058, https://doi.org/10.1016/j.gca.2004.08.020.

Kim J H, Torres M E, Haley B A, Kastner M, Pohlman J W, Riedel M, Lee Y J. 2012. The effect of diagenesis and fluid migration on rare earth element distribution in pore fluids of the northern Cascadia accretionary margin. *Chemical Geology*, **291**: 152-165, https://doi.org/10.1016/j.chemgeo.2011.10.010.

Kim S T, O'Neil J R, Hillaire-Marcel C, Mucci A. 2007. Oxygen isotope fractionation between synthetic aragonite and water: influence of temperature and Mg^{2+} concentration. *Geochimica et Cosmochimica Acta*, **71**(19): 4704-4715, https://doi.org/10.1016/j.gca.2007.04.019.

Kim S T, O'Neil J R. 1997. Equilibrium and nonequilibrium oxygen isotope effects in synthetic carbonates. *Geochimica et Cosmochimica Acta*, **61**(16): 3461-3475, https://doi.org/10.1016/S0016-7037(97)00169-5.

Lawrence M G, Kamber B S. 2006. The behaviour of the rare earth elements during estuarine mixing-revisited. *Marine Chemistry*, **100**(1-2): 147-161, https://doi.org/10.1016/j.marchem.2005.11.007.

Li Y J, Jiang Z L, Liang S, Zhu J Z, Huang Y P, Luan T S. 2016. Hydrocarbon generation in the lacustrine mudstones of the Wenchang Formation in the Baiyun Sag of the Pearl River Mouth Basin, northern South China Sea. *Energy & Fuels*, **30**(1): 626-637, https://doi.org/10.1021/acs.energyfuels.5b02034.

Liang J Q, Wang H B, Su X, Fu S Y, Wang L F, Guo Y Q, Chen F, Shang J J. 2014. Natural gas hydrate formation conditions and the associated controlling factors in the northern slope of the South China Sea. *Natural Gas Industry*, **34**(7): 128-135, https://doi.org/10.3787/j.issn.1000-0976.2014.07.022. (in Chinese with English abstract)

Liang Q Y, Hu Y, Feng D, Peckmann J, Chen L Y, Yang S X, Liang J Q, Tao J, Chen D F. 2017. Authigenic carbonates from newly discovered active cold seeps on the northwestern slope of the South China Sea: constraints on fluid sources, formation environments, and seepage dynamics. *Deep Sea Research Part I*: *Oceanographic Research Papers*, **124**: 31-41, https://doi.org/10.1016/j.dsr.2017.04.015.

Lin Z Y, Sun X M, Strauss H, Eroglu S, Böttcher M E, Lu Y, Liang J Q, Li J, Peckmann J. 2021. Molybdenum isotope

composition of seep carbonates—Constraints on sediment biogeochemistry in seepage environments. *Geochimica et Cosmochimica Acta*, **307**: 56-71, https://doi.org/10.1016/j.gca.2021.05.038.

Lu Y, Sun X M, Lin Z Y, Xu L, Gong J L, Lu H F. 2015. Cold seep status archived in authigenic carbonates: mineralogical and isotopic evidence from Northern South China Sea. *Deep Sea Research Part II*: *Topical Studies in Oceanography*, **122**: 95-105, https://doi.org/10.1016/j.dsr2.2015.06.014.

Lu Y, Sun X M, Xu H F, Konishi H, Lin Z Y, Xu L, Chen T T, Hao X R, Lu H F, Peckmann J. 2018. Formation of dolomite catalyzed by sulfate-driven anaerobic oxidation of methane: mineralogical and geochemical evidence from the northern South China Sea. *American Mineralogist*, **103**(5): 720-734, https://doi.org/10.2138/am-2018-6226.

Magalhães V H, Pinheiro L M, Ivanov M K, Kozlova E, Blinova V, Kolganova J, Vasconcelos C, Mckenzie J A, Bernasconi S M, Kopf A J, Díaz-Del-Río V, González F J, Somoza L. 2012. Formation processes of methane-derived authigenic carbonates from the Gulf of Cadiz. *Sedimentary Geology*, **243-244**: 155-168, https://doi.org/10.1016/j.sedgeo.2011.10.013.

Mazzini A, Svensen H, Hovland M, Planke S. 2006. Comparison and implications from strikingly different authigenic carbonates in a Nyegga complex pockmark, G11, Norwegian Sea. *Marine Geology*, **231**(1-4): 89-102, https://doi.org/10.1016/j.margeo.2006.05.012.

McLennan S M. 1989. Rare earth elements in sedimentary rocks: influence of provenance and sedimentary processes. *In*: Lipin B R, McKay G R eds. Geochemistry and Mineralogy of Rare Earth Elements. De Gruyter, Berlin. p.169-200, https://doi.org/10.1515/9781501509032-010.

Murray R W, Leinen M. 1996. Scavenged excess aluminum and its relationship to bulk titanium in biogenic sediment from the central equatorial Pacific Ocean. *Geochimica et Cosmochimica Acta*, **60**(20): 3869-3878, https://doi.org/10.1016/0016-7037(96)00236-0.

Naehr T H, Eichhubl P, Orphan V J, Hovland M, Paull C K, Ussler III W, Lorenson T D, Greene H G. 2007. Authigenic carbonate formation at hydrocarbon seeps in continental margin sediments: a comparative study. *Deep Sea Research Part II*: *Topical Studies in Oceanography*, **54**(11-13): 1268-1291, https://doi.org/10.1016/j.dsr2.2007.04.010.

Nothdurft L D, Webb G E, Kamber B S. 2004. Rare earth element geochemistry of Late Devonian reefal carbonates, canning basin, Western Australia: confirmation of a seawater REE proxy in ancient limestones. *Geochimica et Cosmochimica Acta*, **68**(2): 263-283, https://doi.org/10.1016/S0016-7037(03)00422-8.

Nozaki Y, Zhang J, Amakawa H. 1997. The fractionation between Y and Ho in the marine environment. *Earth and Planetary Science Letters*, **148**(1-2): 329-340, https://doi.org/10.1016/S0012-821X(97)00034-4.

Nyman S L, Nelson C S, Campbell K A. 2010. Miocene tubular concretions in East Coast Basin, New Zealand: analogue for the subsurface plumbing of cold seeps. *Marine Geology*, **272**(1-4): 319-336, https://doi.org/10.1016/j.margeo.2009.03.021.

Palomares R M, Hernández R L, Frías J M. 2012. Mechanisms of trace metal enrichment in submarine, methane-derived carbonate chimneys from the Gulf of Cadiz. *Journal of Geochemical Exploration*, **112**: 297-305, https://doi.org/10.1016/j.gexplo.2011.09.011.

Paull C K, Hecker B, Commeau R, Freeman-Lynde R P, Neumann C, Corso W P, Golubic S, Hook J E, Sikes E, Curray J. 1984. Biological communities at the Florida Escarpment resemble hydrothermal vent taxa. *Science*, **226**(4677): 965-967, https://doi.org/10.1126/science.226.4677.965.

Paull C K, Ussler III W. 2008. Re-evaluating the significance of seafloor accumulations of methane-derived carbonates: seepage or erosion indicators? *In*: Proceedings of the 6th International Conference on Gas Hydrates (ICGH 2008). Vancouver, British Columbia, Canada.

Peckmann J, Reimer A, Luth U, Luth C, Hansen B T, Heinicke C, Hoefs J, Reitner J. 2001. Methane-derived carbonates and authigenic pyrite from the northwestern Black Sea. *Marine Geology*, **177**(1-2): 129-150, https://doi.org/10.1016/S0025-3227(01)00128-1.

Peketi A, Mazumdar A, Joao H M, Patil D J, Usapkar A, Dewangan P. 2015. Coupled C-S-Fe geochemistry in a rapidly accumulating marine sedimentary system: diagenetic and depositional implications. *Geochemistry*, *Geophysics*, *Geosystems*, **16**(9): 2865-2883, https://doi.org/10.1002/2015GC005754.

Pelejero C, Grimalt J, Heilig S, Kienast M, Wang L J. 1999. High-resolution U^{k}_{37} temperature reconstructions in the South China Sea over the past 220kyr. *Paleoceanography*, **14**(2): 224-231, https://doi.org/10.1029/1998PA900015.

Piper D Z, Calvert S E. 2009. A marine biogeochemical perspective on black shale deposition. *Earth-Science Reviews*, **95**(1-2): 63-96, https://doi.org/10.1016/j.earscirev.2009.03.001.

Raiswell R. 1988. Chemical model for the origin of minor limestone-shale cycles by anaerobic methane oxidation. *Geology*, **16**(7): 641-644, https://doi.org/10.1130/0091-7613(1988)016<0641:CMFTOO>2.3.CO;2.

Reeburgh W S. 2007. Oceanic methane biogeochemistry. *Chemical Reviews*, **107**(2): 486-513, https://doi.org/10.1021/cr050362v.

Roberts H H, Aharon P. 1994. Hydrocarbon-derived carbonate buildups of the northern Gulf of Mexico continental slope: a review of submersible investigations. *Geo-Marine Letters*, **14**(2): 135-148, https://doi.org/10.1007/BF01203725.

Roberts H H, Feng D, Joye S B. 2010. Cold-seep carbonates of the middle and lower continental slope, northern Gulf of Mexico. *Deep Sea Research Part II*: *Topical Studies in Oceanography*, **57**(21-23): 2040-2054, https://doi.org/10.1016/j.dsr2.2010.09.003.

Rongemaille E, Bayon G, Pierre C, Bollinger C, Chu N C,

Fouquet Y, Riboulot V, Voisset M. 2011. Rare earth elements in cold seep carbonates from the Niger delta. *Chemical Geology*, **286**(3-4): 196-206, https://doi.org/10.1016/j.chemgeo.2011.05.001.

Sato H, Hayashi K, Ogawa Y, Kawamura K. 2012. Geochemistry of deep sea sediments at cold seep sites in the Nankai Trough: insights into the effect of anaerobic oxidation of methane. *Marine Geology*, **323-325**: 47-55, https://doi.org/10.1016/j.margeo.2012.07.013.

Schlüter M, Linke P, Suess E. 1998. Geochemistry of a sealed deep-sea borehole on the Cascadia Margin. *Marine Geology*, **148**(1-2): 9-20, https://doi.org/10.1016/S0025-3227(98)00016-4.

Shields G A, Webb G E. 2004. Has the REE composition of seawater changed over geological time? *Chemical Geology*, **204**(1-2): 103-107, https://doi.org/10.1016/j.chemgeo.2003.09.010.

Shields G, Stille P. 2001. Diagenetic constraints on the use of cerium anomalies as palaeoseawater redox proxies: an isotopic and REE study of Cambrian phosphorites. *Chemical Geology*, **17**(1-2): 29-48, https://doi.org/10.1016/S0009-2541(00)00362-4.

Smrzka D, Feng D, Himmler T, Zwicker J, Hu Y, Monien P, Tribovillard N, Chen D, Peckmann J. 2020. Trace elements in methane-seep carbonates: potentials, limitations, and perspectives. *Earth-Science Reviews*, **208**: 103263, https://doi.org/10.1016/j.earscirev.2020.103263.

Stakes D S, Orange D, Paduan J B, Salamy K A, Maher N. 1999. Cold-seeps and authigenic carbonate formation in Monterey Bay, California. *Marine Geology*, **159**(1-4): 93-109, https://doi.org/10.1016/S0025-3227(98)00200-X.

Steinke S, Glatz C, Mohtadi M, Groeneveld J, Li Q Y, Jian Z M. 2011. Past dynamics of the East Asian monsoon: no inverse behaviour between the summer and winter monsoon during the Holocene. *Global and Planetary Change*, **78**(3-4): 170-177, https://doi.org/10.1016/j.gloplacha.2011.06.006.

Su D Q, White N, McKenzie D. 1989. Extension and subsidence of the Pearl River mouth basin, northern South China Sea. *Basin Research*, **2**(4): 205-222, https://doi.org/10.1111/j.1365-2117.1989.tb00036.x.

Su P B, Liang J Q, Peng J, Zhang W, Xu J H. 2018. Petroleum systems modeling on gas hydrate of the first experimental exploitation region in the Shenhu area, northern South China Sea. *Journal of Asian Earth Sciences*, **168**: 57-76, https://doi.org/10.1016/j.jseaes.2018.08.001.

Suess E. 2005. RV SONNE cruise report SO 177, Sino-German cooperative project, South China Sea Continental Margin: geological methane budget and environmental effects of methane emissions and gashydrates. *IFM-GEOMAR Reports*, **4**: 1-154, https://doi.org/10.3289/ifm-geomar_rep_4_2005.

Suess E. 2014. Marine cold seeps and their manifestations: geological control, biogeochemical criteria and environmental conditions. *International Journal of Earth Sciences*, **103**(7): 1889-1916, https://doi.org/10.1007/s00531-014-1010-0.

Sun Q L, Alves T, Xie X N, He J X, Li W, Ni X L. 2017. Free gas accumulations in basal shear zones of mass-transport deposits (Pearl River Mouth Basin, South China Sea): an important geohazard on continental slope basins. *Marine and Petroleum Geology*, **81**: 17-32, https://doi.org/10.1016/j.marpetgeo.2016.12.029.

Taylor S R, McLennan S M. 1985. The Continental Crust: Its Composition and Evolution. Blackwell Scientific Publications, Oxford. p.1-312.

Tong H P, Feng D, Chen D F. 2012. Progresses on petrology, mineralogy and geochemistry of cold seep carbonates in the northern South China Sea. *Journal of Tropical Oceanography*, **31**(5): 45-56, https://doi.org/10.11978/j.issn.1009-5470.2012.05.007. (in Chinese with English abstract)

Tong H P, Feng D, Cheng H, Yang S X, Wang H B, Min A G, Edwards R L, Chen Z, Chen D F. 2013. Authigenic carbonates from seeps on the northern continental slope of the South China Sea: new insights into fluid sources and geochronology. *Marine and Petroleum Geology*, **43**: 260-271, https://doi.org/10.1016/j.marpetgeo.2013.01.011.

Tribovillard N, Algeo T J, Baudin F, Riboulleau A. 2012. Analysis of marine environmental conditions based onmolybdenum-uranium covariation—applications to Mesozoic paleoceanography. *Chemical Geology*, **324-325**: 46-58, https://doi.org/10.1016/j.chemgeo.2011.09.009.

Tribovillard N, Algeo T J, Lyons T, Riboulleau A. 2006. Trace metals as paleoredox and paleoproductivity proxies: an update. *Chemical Geology*, **232**(1-2): 12-32, https://doi.org/10.1016/j.chemgeo.2006.02.012.

Turekian K K, Wedepohl K H. 1961. Distribution of the elements in some major units of the Earth's crust. *GSA Bulletin*, **72**(2): 175-192, https://doi.org/10.1130/0016-7606(1961)72[175:DOTEIS]2.0.CO;2.

Warren J. 2000. Dolomite: occurrence, evolution and economically important associations. *Earth-Science Reviews*, **52**(1-3): 1-81, https://doi.org/10.1016/S0012-8252(00)00022-2.

Wu N Y, Yang S X, Zhang H Q, Liang J Q, Wang H B, Lu J A. 2010. Gas hydrate system of Shenhu area, northern South China Sea: wire-line logging, geochemical results and preliminary resources estimates. *In*: Paper presented at the Offshore Technology Conference. OTC, Houston, Texas, USA. https://doi.org/10.4043/20485-MS.

Xie X N, Müller R D, Li S T, Gong Z S, Steinberger B. 2006. Origin of anomalous subsidence along the northern South China Sea margin and its relationship to dynamic topography. *Marine and Petroleum Geology*, **23**(7): 745-765, https://doi.org/10.1016/j.marpetgeo.2006.03.004.

Yang K H, Chu F Y, Zhu Z M, Dong Y H, Yu X G, Zhang W Y, Ma W L. 2018. Formation of methane-derived carbonates during the last glacial period on the northern slope of the South China Sea. *Journal of Asian Earth Sciences*, **168**: 173-185, https://doi.org/10.1016/j.jseaes.2018.01.022.

Yu H S. 1990. The Pearl River Mouth Basin: a rift basin and its geodynamic relationship with the southeastern Eurasian margin. *Tectonophysics*, **183**(1-4): 177-186, https://doi.

org/10.1016/0040-1951(90)90415-5.

Zhang F F, Xu H F, Konishi H, Kemp J M, Roden E E, Shen Z Z. 2012. Dissolved sulfide-catalyzed precipitation of disordered dolomite: implications for the formation mechanism of sedimentary dolomite. *Geochimica et Cosmochimica Acta*, **97**: 148-165, https://doi.org/10.1016/j.gca.2012.09.008.

Zhang H Q, Yang S X, Wu N Y, Schultheiss P, GMGS-1 Science Team. 2007. China's first gas hydrate expedition successful. *Fire in the Ice*: *Methane Hydrate Newsletter*, **7**(2): 4-8, https://netl.doe.gov/sites/default/files/publication/HMNewsSpringSummer07.pdf. Accessed on 2021-04-18.

Zhang W, Liang J Q, Lu J A, Wei J G, Su P B, Fang Y X, Guo Y Q, Yang S X, Zhang G X. 2017. Accumulation features and mechanisms of high saturation natural gas hydrate in Shenhu Area, northern South China Sea. *Petroleum Exploration and Development*, **44**(5): 708-719, https://doi.org/10.1016/S1876-3804(17)30082-4.

Zhang W, Liang J Q, Su P B, Wei J G, Sha Z B, Lin L, Liang J, Huang W. 2018. Migrating pathways of hydrocarbons and their controlling effects associated with high saturation gas hydrate in Shenhu area, northern South China Sea. *Geology in China*, **45**(1): 1-14, https://doi.org/10.12029/gc20180101. (in Chinese with English abstract)

Zhang W, Liang J Q, Wei J G, Su P B, Lin L, Huang W. 2019. Origin of natural gases and associated gas hydrates in the Shenhu area, northern South China Sea: results from the China gas hydrate drilling expeditions. *Journal of Asian Earth Sciences*, **183**: 103953, https://doi.org/10.1016/j.jseaes.2019.103953.

Zhao M X, Huang C Y, Wang C C, Wei G J. 2006. A millennial-scale $U_{37}^{K'}$ sea-surface temperature record from the South China Sea (8°N) over the last 150 kyr: monsoon and sea-level influence. *Palaeogeography*, *Palaeoclimatology*, *Palaeoecology*, **236**(1-2): 39-55, https://doi.org/10.1016/j.palaeo.2005.11.033.

Zheng Y, Anderson R F, Van Geen A, Fleisher M Q. 2002. Preservation of particulate non-lithogenic uranium in marine sediments. *Geochimica et Cosmochimica Acta*, **66**(17): 3085-3092, https://doi.org/10.1016/S0016-7037(01)00632-9.